minerals

MDPI

Article

The Caudofoveata (Mollusca) Spicule as a Biomineralization Model: Unique Features Revealed by Combined Microscopy Methods

Camila Wendt [1], André L. Rossi [2], Jefferson Cypriano [3], Cleo Dilnei de Castro Oliveira [4], Corinne Arrouvel [5], Jacques Werckmann [2] and Marcos Farina [1,*]

1 Instituto de Ciências Biomédicas, Universidade Federal do Rio de Janeiro, Rio de Janeiro 21941-590, Brazil; camilacwendt@gmail.com
2 Centro Brasileiro de Pesquisas Físicas, Rio de Janeiro 22290-180, Brazil; alinhares@cbpf.br (A.L.R.); j.werckmann@gmail.com (J.W.)
3 Instituto de Microbiologia, Universidade Federal do Rio de Janeiro, Rio de Janeiro 21941-590 Brazil; jeffcy@micro.ufrj.br
4 Instituto de Biologia, Universidade Federal do Rio de Janeiro, Rio de Janeiro 21941-590, Brazil; cleo.oliveira@gmail.com
5 Centro de Ciências e Tecnologia para a Sustentabilidade, Departamento de Física, Química e Matemática, Universidade Federal de São Carlos, São Paulo 13565-905, Brazil; corinne@ufscar.br
* Correspondence: marcos.farina.souza@gmail.com

Abstract: Caudofoveates are benthic organisms that reside in the deep waters of continental slopes in the world. They are considered to be a group that is of phylogenetic and ecological importance for the phylum Mollusca. However, they remain poorly studied. In this work, we revealed the structure of the spicules of Caudofoveatan mollusks *Falcidens* sp. The spicules presented a hierarchical organization pattern across different length scales. Various imaging and analytical methods related to light and electron microscopy were employed to characterize the samples. The primary imaging methods utilized included: low voltage field emission scanning electron microscopy (FEG-SEM), focused ion beam-scanning electron microscopy (FIB-SEM), high-resolution transmission electron microscopy (HRTEM), atomic force microscopy (AFM), and electron diffraction. In addition, we performed a physicochemical analysis by electron energy loss spectroscopy (EELS) and energy dispersive X-ray spectroscopy (EDS). A crucial factor for successfully obtaining the results was the preparation of lamellae from the spicules without damaging the original structures, achieved using FIB-SEM. This allowed us to obtain diffraction patterns of significant areas of well-preserved sections (lamellae) of the spicules in specific directions and demonstrate for the first time that the bulk of these structures is organized as a single crystal of calcium carbonate aragonite. On the other hand, AFM imaging of the spicules' dorsal surface revealed a wavy appearance, composed of myriads of small, pointed crystallites oriented along the spicules' longer axis (i.e., the *c*-axis of the aragonite). The organization pattern of these small crystallites, the possible presence of twins, the relationship between confinement conditions and accessory ions in the preference for mineral polymorphs, and the single crystalline appearance of the entire spicule, along with the observation of growth lines, provide support for further studies employing Caudofoveata spicules as a model for biomineralization studies.

Keywords: aragonite; nanostructure; biomineralization; low-voltage FEG-SEM; scanning probe microscopy; FIB-SEM; Caudofoveata

Citation: Wendt, C.; Rossi, A.L.; Cypriano, J.; Dilnei de Castro Oliveira, C.; Arrouvel, C.; Werckmann, J.; Farina, M. The Caudofoveata (Mollusca) Spicule as a Biomineralization Model: Unique Features Revealed by Combined Microscopy Methods. *Minerals* **2023**, *13*, 750. https://doi.org/10.3390/min13060750

Academic Editors: Yannicke Dauphin, Fabio Nudelman and Jean-Pierre Cuif

Received: 28 March 2023
Revised: 15 May 2023
Accepted: 26 May 2023
Published: 31 May 2023

1. Introduction

Mollusks have been widely used as models for studies of biomineralization mechanisms [1,2]. Early analyses of mollusk shell microstructure relied on light microscopy [3]. After the 1960s, electron microscopy emerged as an important tool in determining shell microstructure [4]. Over the past few decades, innovative imaging methods and advances

in physicochemical methods provided greater opportunities for obtaining structural information on biominerals [5–8].

In Caudofoveata, a class of marine worm-like infaunal mollusks without a shell or plates, the soft body is covered by calcareous spicules embedded in a chitinous cuticular layer. The spicules are formed extracellularly within a deep invagination of a single cell, where calcium carbonate is secreted onto a cup-like organic template [9,10]. The morphology, size, and thickness of the spicules can differ along the body regions, which are typically characterized by smaller and broader spicules at the anterior region [11]. The pattern of spicule diversity along the body has been considered species-specific and is largely used in systematics, e.g., [12–14]. Despite their importance, the structure and growth patterns of the mineral hard parts of the Caudofoveatan spicules have been poorly studied and are still being documented.

Caudofoveatan spicules have been thought to be aragonitic [15]. However, despite advances in the study of sclerite development (see Kingsley et al., [16], for a historical overview), there is no detailed account of the Caudofoveata spicule composition and crystallography.

Here, we investigated the spicule architecture, texture pattern, and microstructure of Caudofoveata mollusks *Falcidens* sp. using light microscopy, low-voltage field emission scanning electron microscopy (low-voltage FEG-SEM), focused ion beam (FIB) associated with scanning electron microscopy (SEM) and electron diffraction techniques. Atomic force microscopy (AFM) was used as a complementary technique to describe the topography of spicule surfaces. Employing these techniques in a combined manner allowed for a fine characterization of Caudofoveatan spicules. The spicules exhibited plate-like alternating substructures oriented in parallel at the micrometer scale. At the nanometer scale, electron diffraction revealed that the bulk of the spicule corresponds to a single crystal of aragonite.

2. Materials and Methods

2.1. Samples

Falcidens sp. specimens were obtained from the Malacological Collection of the Biological Institute of the Federal University of Rio de Janeiro (IBUFRJ) (Rio de Janeiro, Brazil). Briefly, samples were collected in 1986, between 25 and 97 m deep, on the continental slope (22°55′ S, 42°00′ W and 23°05′ S, 42°20′ W) of Rio de Janeiro State, Brazil. Specimens were immediately fixed in buffered 4% formaldehyde for 24 h and preserved in 70% ethanol at the collection.

2.2. Polarized Light Microscopy (PLM) and Nomarski Differential Interference Contrast (DIC)

Spicules (obtained mainly from the middle region of the animal) were rinsed in distilled water, washed in xylol, mounted on glass slides with synthetic balsam (Entellan; Merck), and observed with a Zeiss Axiophot microscope (Carl Zeiss, Oberkochen, Germany) equipped with a rotatable stage, fixed crossed polarizers, and Nomarski differential interference contrast (DIC). Images were captured using a video camera (SIT) attached to the microscope. IBAS software (version 2.0, Kontron-Zeiss, Eching, Germany) was used to capture and analyze the images that were digitally filtered using the Fast Fourier Transform (FFT) routine.

2.3. Reflected Light Microscopy

The spicules were deposited on glass slides and sputtered with gold (~30 nm), and observed with a Zeiss Axiophot reflected light microscope equipped with optical accessories for Nomarski DIC and dark field reflected light microscopy, using a 50× planachromatic objective lens.

2.4. Scanning Electron Microscopy (SEM) and Field Emission Scanning Electron Microscopy (FEG-SEM)

Spicules were extensively washed in distilled water, air-dried, and mounted on silicon chip specimen supports. The supports were placed on aluminum stubs and slightly coated (~5 nm) with chromium in a high-resolution sputter coater (Gatan 681 High Resolution Ion Beam Coater, Gatan Inc., Pleasantown, CA, USA). The specimens were imaged with secondary electrons in a Jeol 6340 FEG-SEM (JEOL Ltd., Akishima, Japan) operated at accelerating voltages ranging from 1 to 20 kV. Some isolated spicules were cleaned in a 5% NaOH solution for 10 min and 10% NaOH for 30 min to eliminate the organic components from the surface. For acid digestion, a 0.02 M citric acid solution was used to etch the crystalline calcium carbonate phase for 5 to 10 min; the spicules were washed in deionized water and processed for SEM analysis.

2.5. High-Resolution Transmission Electron Microscopy (HRTEM), Electron Diffraction, Electron Energy Loss Spectroscopy (EELS), and Energy Dispersive X-ray Spectroscopy (EDS)

Samples were prepared in a TESCAN Lyra 3 (TESCAN, Brno, Czech Republic) dual beam (Ga^+ and electron beam) by in situ lift-out technique. The spicules were embedded in an epoxy resin with their axis approximately parallel to the surface, polished, and coated with a 10 nm thin gold layer for surface protection and electrical conductivity. In the dual beam, the spicule was covered with a 1 µm Pt layer. The lamella was thinned up to 1 µm with a 30 kV/0.1 nA (probe current, unit nA) Ga (Gallium) probe, for thicknesses between 1 µm and 200 nm, using a 10 kV/0.1 nA probe from 200 nm to 70 nm, with a 5 kV/0.01 nA probe.

Transmission electron microscopy (TEM) analysis was performed in JEOL 2100F equipment (JEOL Ltd., Akishima, Japan) operated at 200 kV. The microscope was equipped with a CMOS Camera 4K × 4K (One View—Gatan, Gatan Inc., Pleasantown, CA, USA), an EELS filter (Tridiem—Gatan, Gatan Inc., Pleasantown, CA, USA), and an EDS detector (Xplore 80 mm^2—Oxford, Oxford Instruments, Abingdon, UK). EELS was acquired in scanning transmission electron microscopy (STEM) mode with an energy resolution of approximately 1.5 eV. Selected area electron diffraction (SAED), was obtained using selected area apertures in TEM mode (parallel beam). A double tilt holder (Gatan) was used to orient the sample in a low-index zone axis. Diffraction patterns were compared to simulated patterns from calcite, aragonite, and vaterite calcium carbonate polymorph phases using Java electron microscopy software (JEMS, version V4, Jems-swiss, Jongny, Switzerland).

2.6. Atomic Force Microscopy

Samples were imaged using a Topometrix Accurex II (Topometrix, Santa Clara, CA, USA) instrument, equipped with a contact AFM probe head and a 100 µm Tripot scanner. The silicon tips (Topometrix 1660e) were mounted on a cantilever with a spring constant of ca. 40 N/m and resonance frequencies in the 100–150 kHz range. The samples were fixed on the slide with a thin gelatin layer. Three-dimensional graphics and profile measurements were computer generated using the Topometrix Software (Topometricx SPMLab NT Ver.5.0, ThermoMicroscopes, Sunnyvale, CA, USA). Alternatively, a Nanoscope III atomic force microscope was used with similar tips and observation conditions.

3. Results

3.1. Structure

Falcidens sp.'s body is decorated by tightly packed overlapping spicules forming a longitudinal striation pattern (Figures 1a and S1). Scanning electron microscopy images showed that the oral shield spicules are attached to the tegumentum of *Falcidens* sp. by a chitinous cup-like base (Figure 1b). Transmitted DIC-Normaski microscopy of longitudinal semi-thin sections of the organism showed that the tegumentum of *Falcidens* sp. is composed of a cuticle containing the calcareous spicules (Figure 2a). The spicules are made of

two parts: the base inserted in the cup-like organic base (Figures 1b and 2a, arrow) and a blade extending beyond the cup-like base.

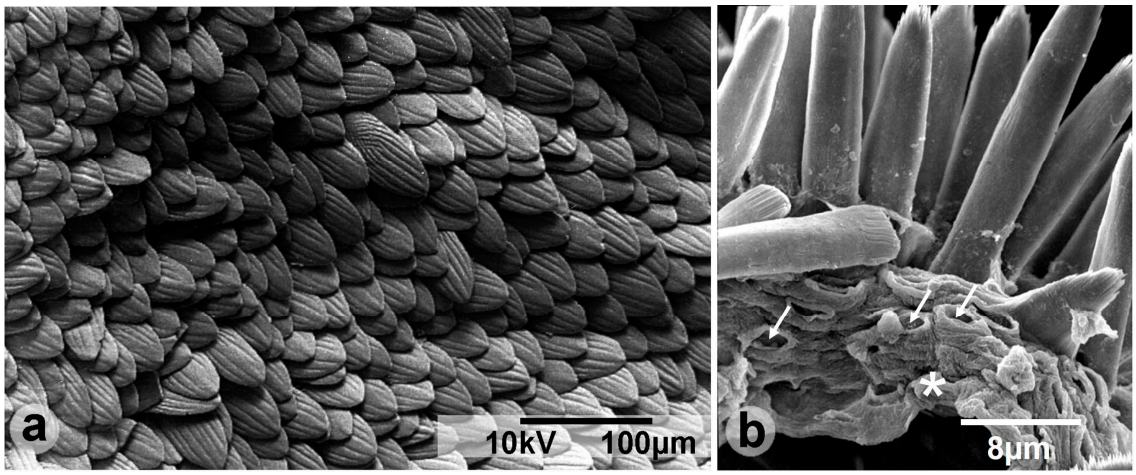

Figure 1. The morphology of the spicules of *Falcidens* sp. (**a**) SEM image showing the spicules attached in the tegumentum; (**b**) SEM image showing elongated spicules attached in the chitinous cup-like base. Asterisk: tegumentum; arrows: cup-like base.

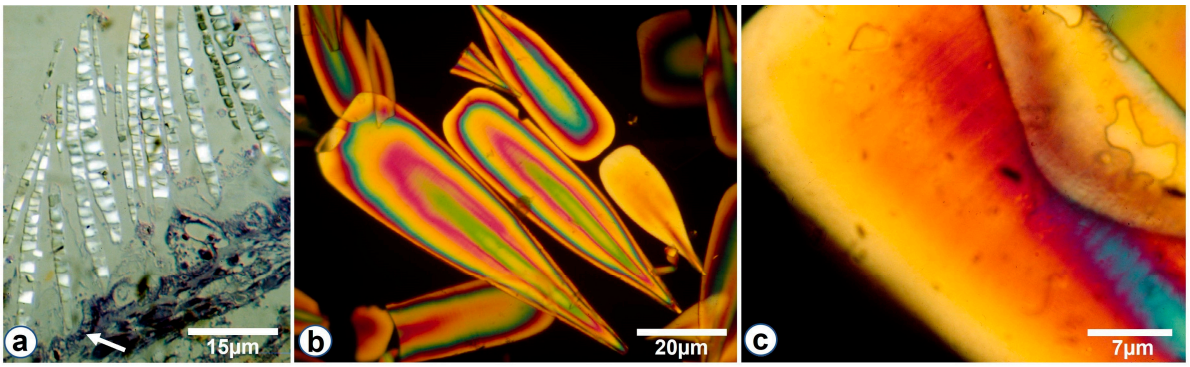

Figure 2. Details of spicules by light microscopy. (**a**) Polarized light microscopy image of an anterior (sagittal to the organism's body) longitudinal section of the body showing the spicules attached in the organic cup (arrow); (**b**) Polarized light microscopy of the spicules showing the symmetrical birefringent isochromes. In this image, the polarizer is oriented parallel to the X (horizontal) axis while the analyzer is parallel to the Y (vertical) axis. Most spicules in the field were oriented at 45° and showed maximum brightness; (**c**) Higher magnification of the polarized light microscopy image, showing the birefringent isochromes and faint parallel lines running perpendicular to the main axis of the spicule.

Observation of the isolated spicules by polarization light microscopy showed that they have birefringent properties. Of note is that the continuous distribution of interference colors indicated that each spicule behaved as a single crystal (Figure 2b). Differences in thickness caused a longitudinal isochrome symmetry of the spicule when examined under crossed polarizers. The thicker part of the spicules was at the center, and the thickness decreased continuously from the center to the extremities of the spicules (particularly the pointed end). Most spicules were about 90 nm in length, symmetrical, and curved slightly toward the body. The images (Figure 2b) are compatible with the interpretation that the longer axis of the spicules was the c-symmetry axis of the crystals, which, in this case, were made of aragonite (see later in this section). Closer examination (Figure 2c) showed a series of parallel lines running perpendicular to the main axis of the spicule.

Reflection Nomarski interference contrast light microscopy revealed differences in surface texture between both sides of the spicules. The part of the spicule facing the

environment (distal side) was curved (convex) and composed of interlaced undulations that protruded from the surface of the spicule (Figure 3a). In contrast, the part of the spicule facing the mollusk body (proximal side) was flat and presented periodicity lines (growth lines) perpendicular to the spicule axis (Figure 3b). The lines became more evident after 0.02 M citric acid bath of the spicules (Figure 3c) and this was further confirmed by Fast Fourier Transform filtration, also evidenced by the existence of thick and thin lines in the transmitted DIC (Figure 3d).

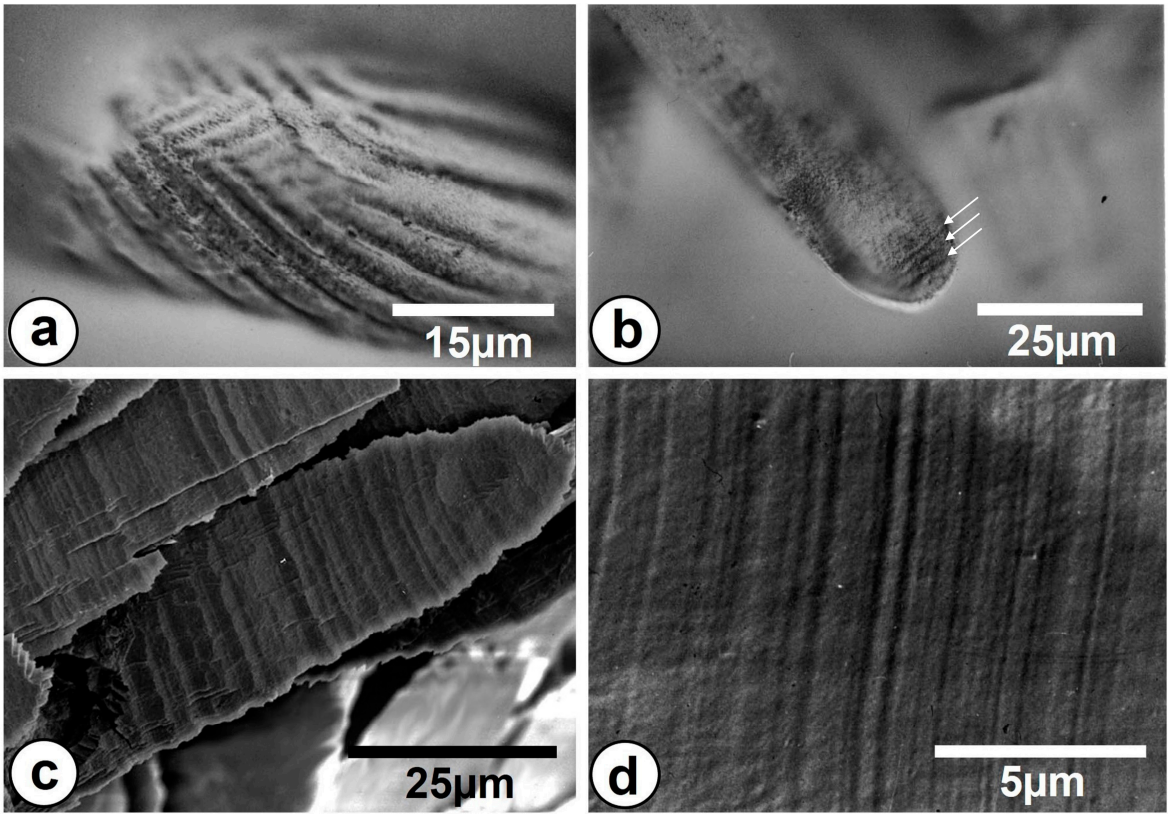

Figure 3. Topography of the surface of spicules by differential interference contrast/reflected light (DIC/RL) image of gold sputtered spicules. (**a**) DIC/RL of the dorsal face showing the presence of chevron-like ornamentation (undulations) and small crystallites emerging from the ornamentation (Supplementary Materials Figures S2–S4); (**b**) DIC/RL image showing the striations (growth lines) perpendicular to the longer axis of the ventral face of spicules and presenting a smoother texture; (**c**) SEM image showing lines of the acid-treated ventral face of spicules, arranged perpendicularly to the longer axis. Lines have different thicknesses and different distances among them; (**d**) Detail of the lines shown in Figure 3c. Arrows in (**b**): striations.

3.2. Micro- and Nanostructures

The bases of the spicules showed numerous fine, evenly spaced, longitudinal ridges, which also sometimes appeared on the blades. The untreated spicules observed at low-voltage SEM (3.5 kV) displayed a similar texture when observed under reflective Nomarski differential interference contrast light microscopy (DIC/RL). However, the ventral side exhibited a granular texture and did not show periodicity lines, as seen in the light microscopy images. The NaOH-treated spicules revealed mesolayers parallel to the longitudinal axis at the base (Figure 4a). The platinum replica (Figure 4a, inset) of the spicule base treated in 5% NaOH (Figure 4b) showed that the mesolayers contained layers about 400 nm thick. Higher magnification SEM images (Figure 4b) evidenced that in this region, the treated surface is formed by alternating parallel layers of "smooth" and "rough" texture.

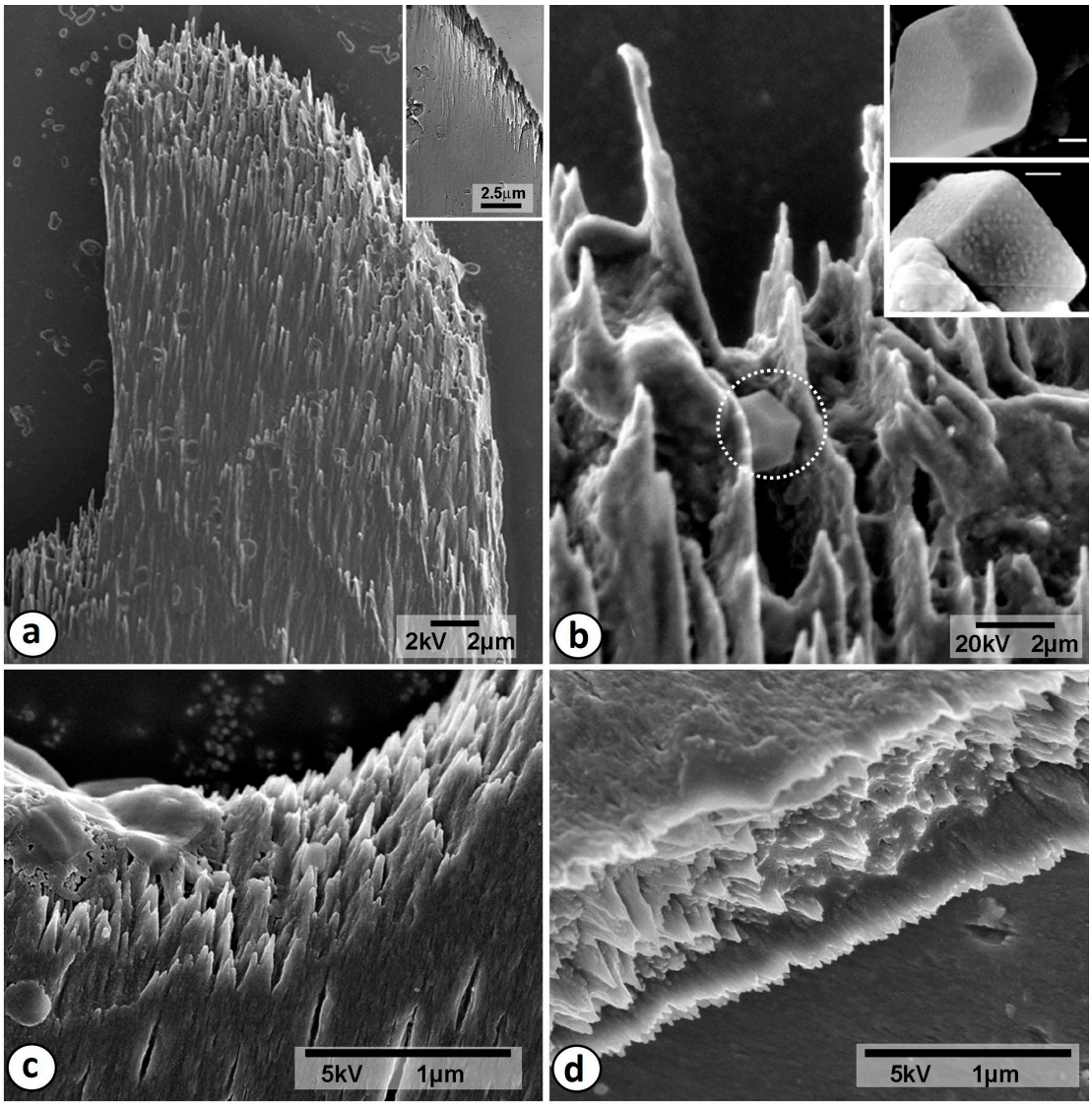

Figure 4. (**a**) Low-voltage FEG-SEM image of the base of an alkali-treated spicule displaying sheet-like structures showing sharp profiles. Inset shows a freeze-fractured replica of treated (5% NaOH) spicule. The white lines in the replica correspond to the thickness of the mesolayer (~400nm); (**b**) High magnification from a region depicted in (**a**). Note the layered organization of the structure. Small crystal-like particles were sometimes present, possibly indicating a reprecipitation. Bars: 350 nm (upper insert) and 300 nm (lower insert); (**c**) End base view of a spicule showing end sharp crystals; (**d**) Internal structure of spicule, broken at its base and displaying pointed sharp crystals with variable angles.

Single crystal-like particles (dotted circle in Figure 4b, upper and lower insets in this figure) were occasionally seen between the mesolayers. The treatment of the spicule base with 5% NaOH also revealed that bundles of pointed crystals composed one of the layers (the "rough" one), as indicated in Figure 4c. A fragment of a broken untreated spicule base (Figure 4d) showed several pointed crystals embedded in a material with a smooth topography.

Low-voltage SEM imaging of the spicule blades treated with 5% NaOH revealed the presence of crystal tablets oriented perpendicular to the spicule surface (Figure 5a,b). The 10% NaOH-treated blades displayed tightly packed tablets running parallel to the longitudinal axis (Figure 5c), with variable lengths. High-magnification SEM images of 0.02 M citric acid-treated spicule bases revealed the presence of two types of structures:

thin layers about 50 nm thick, separated by layers of a material with a smooth topography about 200 nm thick (Figure 5d).

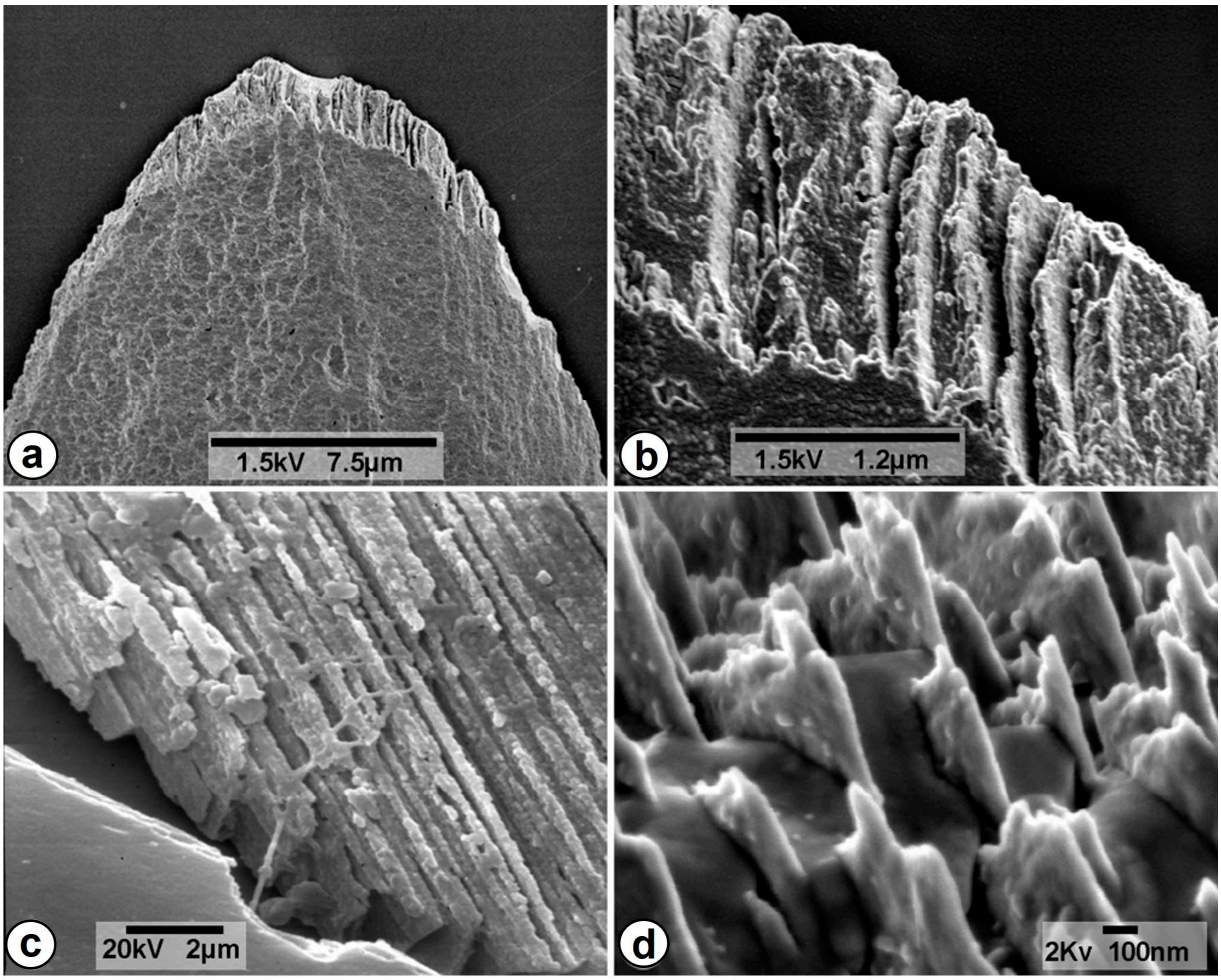

Figure 5. (**a**) SEM image of end blade region (tip of the spicule) showing layers of crystals aligned in parallel and perpendicular to the spicule surface; (**b**) High magnification from a region depicted in (**a**). Detail of the region composed of parallel layers. Note that the layers are regularly spaced; (**c**) Highly alkali-etched spicule displaying alternating layers, disposed in parallel to each other; (**d**) Acid-treated base of the spicule showing regions of different textures. These regions may have different compositions and/or different mineral/organic ratios.

3.3. Surface Morphology of Spicules by AFM

Selected areas of the distal and proximal surfaces of untreated spicules were measured by AFM. The distal surface of the spicule (Figure 6a) exhibited ripple-like lines, which intersected at an angle of about 58° (Figure 6b). The surface of the region depicted in Figure 6a showed the ectopic crystallites growing obliquely to the main axis of the ripples (Figure 6d), but parallel to the symmetry axis of the spicule. Upon closer examination, the ectopic crystallites could be seen emerging from the crossed surface (Figure 6c). The height map of ectopic crystallite remnants ranged from 223 to 447 nm (Figure 6e). Higher magnification AFM analysis provided details on the topography of the crystallite distribution on the spicule dorsal side (see Supplementary Materials, Figures S1 and S2). Crystallites ran parallel in the direction of the spicule´s axis, in a wavy pattern, with a maximum amplitude of about 200 nm (Figure S1). On the other hand, the top surface of the crystals was approximately the same height as that of the neighbors on a section plane perpendicular to the longer axis of the spicule (Figure S2). Supplementary Materials, Figure S3 and Table S1, show that the crystallites were oriented in the *c*-axis direction of the aragonite crystal.

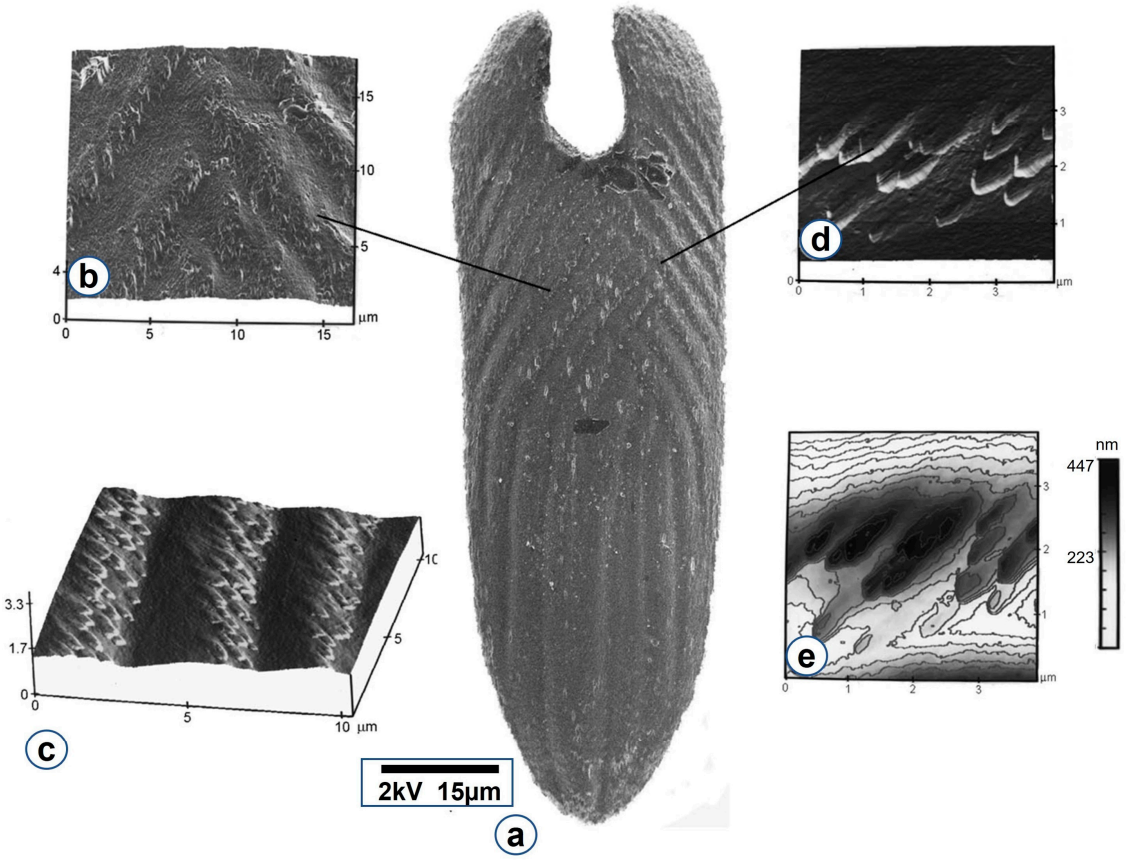

Figure 6. Composite plate showing the topology and crystallographic properties of the distal face of the spicules imaged with AFM and low-voltage FEG-SEM. (**a**) Distal face of spicule, displaying crystallites emerging from the spicule surface; (**b**) AFM image (contact mode in air) from a region depicted in (**a**). The chevron-like structures are clearly visible; (**c**) AFM image (contact mode in air) from a region depicted in (**a**). Observe the superimposed crystals emerging from the spicule surface; (**d**) Topological measurement of Figure 3e, showing the height of the acicular crystallites; (**e**) AFM image of the acicular crystallites displaying an average angle of 88°.

The proximal side of the spicules (Figure 7a) exhibited a smooth surface when imaged by FEG-SEM, but a rough surface, with crystalline regions separated by thin less crystalline dark layers (Figure 7b), when imaged by AFM. The frictional images showed that the contour of each particle presented more viscosity than the bulk region (Figure 7c). This type of organization of parallel lines is compatible with what appears in Figure 3c,d, strengthening the hypothesis that the mineral content is anisotropically distributed inside the bulk of the material.

The spicule lamellae obtained by FIB-SEM presented a homogeneous contrast when observed by low magnification TEM (Supplementary Materials, Figure S5a). HRTEM images of the lamella revealed continuous lattice fringes, indicating that the analyzed regions behaved as a single crystal (Supplementary Materials, Figure S5b). We also acquired SAED patterns using a double tilt holder to orient the lamella in a low Miller index (Supplementary Materials, Figure S6). We then compared the diffraction patterns shown in Figure 8a with calcite, aragonite, and vaterite crystalline structures. The only possible solution is presented in Figure 8b. The diffraction pattern was indexed in the [001] zone axis of aragonite. Note that the most internal diffracted spots (020, 0–20, 110, −1–10, −110, and 1–10) did not form a perfect hexagonal pattern. The spacing between (020) lattice planes was a little bit smaller (0.42 nm) than the (110) and (1–10) planes (0.44 nm). The 020 and 200 vectors presented an angle of 90°, compatible with the orthorhombic system.

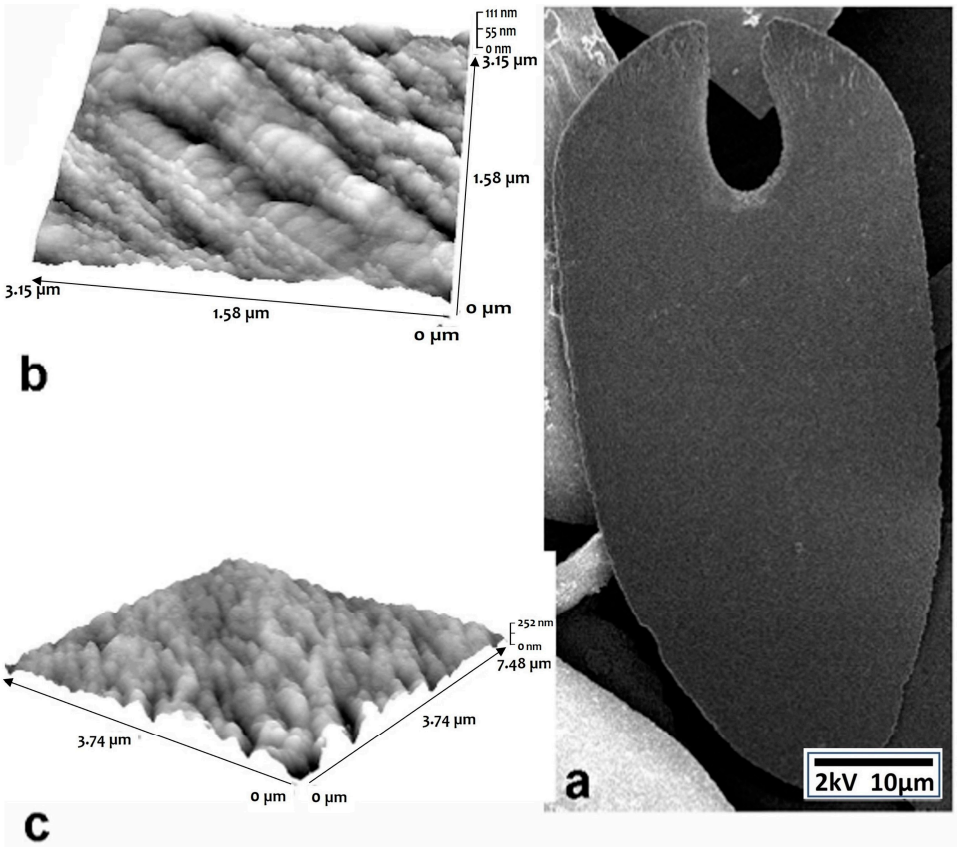

Figure 7. Composite plate showing the topography and crystallographic properties of the proximal face of the spicules imaged with low-voltage FEG-SEM and AFM. (**a**) Proximal face of spicule, displaying a smoother surface; (**b**) Frictional image where the contours of each particle present more viscosity from that bulk region. This type of parallel distribution in parallel lines is compatible with what appears in Figure 3c,d; (**c**) AFM image (contact mode in air) from the surface displaying rounded particles with variable morphology and dimension. Note that the image in (**c**) is rotated in relation to (**b**).

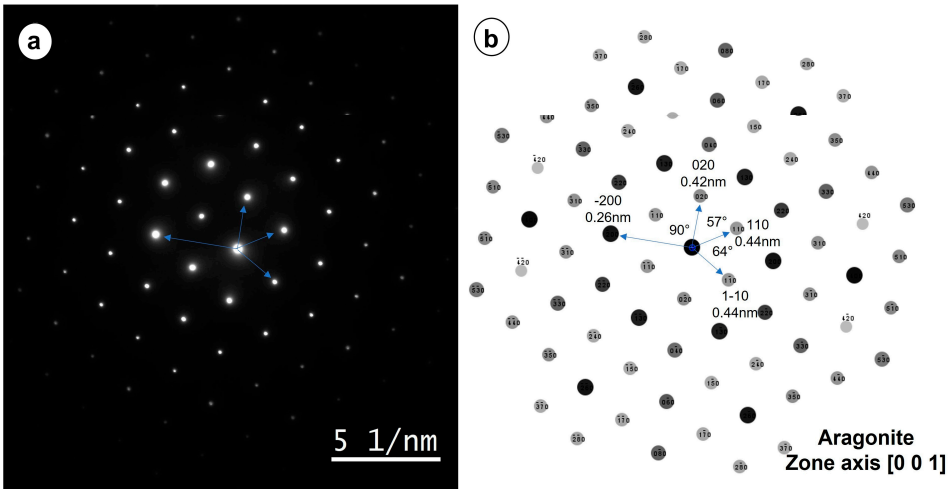

Figure 8. Crystallographic characterization of spicules by analyzing a lamella obtained by FIB-SEM. (**a**) Diffraction pattern from a spicule lamella perpendicular to the longer axis of the spicule; (**b**) Idealized model of aragonite observed along the [001] zone axis. Note that both distances and angles between lattice planes corresponded to what would be expected from the aragonite crystal structure.

3.4. Electron Energy Loss Spectroscopy (EELS) and Energy Dispersive X-ray Spectroscopy (EDS)

Next, we analyzed the lamella by EELS, using the scanning transmission electron microscopy mode. We detected carbon K edge, calcium L edge, and oxygen K edge at 290, 350, 530 eV energy losses, respectively (Figure 9a,b). The carbon edge was typical of carbonate (CO_3) bonding sites, presenting one narrow peak at 290 eV and one broader peak at 300 eV, assigned to C=O ($1s \rightarrow \pi^*$) and C–O ($1s \rightarrow \sigma^*$) bonds of the carbonate group, respectively. We also observed a small pre-peak (285 eV) before these two more intense peaks, which may have been due to a small amount of amorphous carbon. The spectrum from amorphous carbon presented a small peak at 285 eV ($1s \rightarrow \pi^*$) and a large broad peak at 295 eV ($1s \rightarrow \sigma^*$). Spectra were obtained in different regions of the lamella and did not vary, suggesting no compositional variation along the sample. The energy loss near-edge structure of oxygen (Figure 9b) from the sample, showed similarity with what is described in the work of Srot et al. [17] for biogenic aragonite crystals.

We also performed an elemental analysis of a spicule by energy dispersive X-ray spectroscopy (EDS) in a JEOL 2100F HRTEM. Strontium and sulfur were also detected from the aragonite mineral, besides carbon, oxygen, and calcium elements (Figure 10). These findings allowed for a discussion of the characteristics of aragonite in association with Sr and the possible role of sulfur in contributing to the determination of the calcium carbonate polymorph. For considerations on this subject see the Section 4 below.

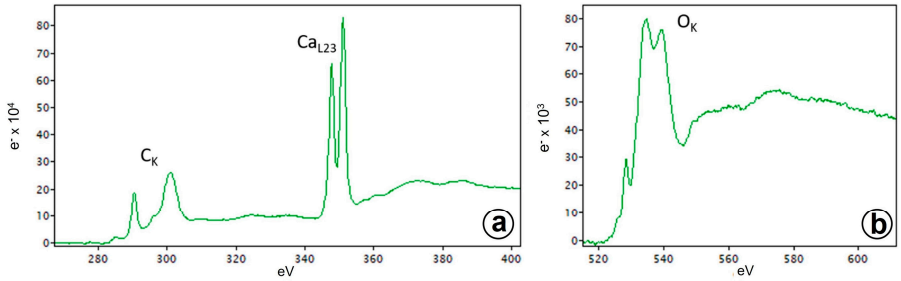

Figure 9. EELS spectrum obtained from a lamella prepared by FIB. (**a**) Energy loss from 270 to 400 eV; (**b**) Energy loss from 520 to 610 eV. The backgrounds from spectra A and B were subtracted. The two peaks at ~300 eV energy loss corresponded to the carbon edge, peaks at 350 eV corresponded to the $CaL_{2,3}$ edge, and peaks at 530 eV corresponded to the O-K edge. The spectrum is typical of calcium carbonate with probably no organic matter or a very low content of organic matter. This information was obtained by the "energy loss near-edge structure" for the carbon, which is typical of crystalline calcium carbonates (see the main text for numerical details).

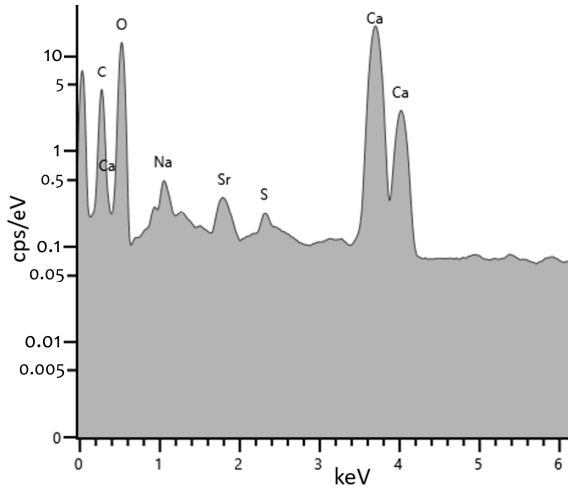

Figure 10. Elemental composition of a spicule lamella obtained by energy dispersive X-ray analysis (EDS). Peaks corresponding to calcium carbonate (C, O, and Ca) are easily seen. Additionally, Na, Sr, and S were detected.

4. Discussion

The formation of hard biological materials, i.e., bone, shell, and otoconia, typically involves the deposition of specific inorganic minerals on or within an organic matrix, in a highly controlled manner [2,7]. Control over biomineralization is one of the most striking features of biological organisms [18]. It is assumed that the presence of organic matter in biominerals can precisely direct the organization of the inorganic crystalline parts during the synthesis of a biomineral composite [19–21]. Thus, understanding the molecular organization of a composite structure such as spicules is crucial for understanding their biophysical properties. The structural attributes of a biomineral provide information on their formation and possibly the evolution pattern of the biomineralization process [2,22].

We believe that the present work will contribute to encouraging further studies on Caudofoveata spicules. To a large extent, the works in the literature on the description of spicules of this group of organisms are focused on aspects of phylogeny and not on the structure of the material. For this reason, possibly, morphological data obtained from stereoscopic magnifying glasses, polarization light microscopy, or SEM have been considered sufficient. However, as we have shown here, due to the richness of the structural details, and the questions brought to light, spicules may become an important model for biomineralization studies. To this end, the methods used here and the cooperation between researchers from different fields, such as physics, materials science, and biology, will be fundamental.

In this work, we used FIB-SEM to produce spicules lamellae oriented perpendicularly to their longer axis and showed that these regions behaved as single crystals of aragonite. However, SEM images of NaOH or acid-treated spicules indicated that the bulk of these regions is composed of a set of alternating thinner, most likely crystalline, components, oriented in parallel, with different textures. This is an intriguing result, as a combination of HRTEM, electron diffraction and EELS suggested a monocrystalline calcium carbonate material, whereas SEM images presented it as a biocomposite with different structures combined in the bulk.

Therefore, it would be of great interest to study the structures and composition of the two individual regions in detail with nanoscale imaging techniques, with an emphasis on their interfaces. This proposed issue is of paramount importance for the subject of biomineralization, highlighting the significance of this study model moving forward.

The various techniques we used in a combined manner to study *Falcidens* sp. spicules allowed the characterization of different organization patterns at different length scales. From polarization light images, SEM, AFM, and high-resolution analytical TEM, we were able to characterize:

1. The macroscopic shape and optical behavior of spicules: they appeared to present a single crystalline structure. We also observed some faint lines oriented perpendicular to the longer axis (usually considered as growth lines), which calls for a deeper analysis.
2. The wavy pattern of the dorsal face of spicule using reflection light microscopy images at the same length scale.
3. The micrometer-sized needle-like crystallites composing the ridge of the wavy topography using FIB-SEM with low voltage at a higher magnification.
4. The morphology of individual needle-like crystallites using AFM at the submicrometer level. We evidenced their suggested oblique faces exposed at the tip and the association of crystallites with their neighbors.
5. The presence of layers of plate-like alternating crystals aligned in parallel and perpendicular to the spicule´s surface, as observed by SEM of acid- and alkali-treated spicules.
6. The spicules as aragonite with the *c*-axis oriented in the direction of the longer axis using electron diffraction of spicules lamellae oriented perpendicular to their longer axes. To our knowledge, this result is being shown for the first time.

We used electron energy loss spectroscopy (EELS) in STEM mode to evaluate the energy loss near-edge structure of the carbon edge in spicules lamellae. The carbon edge

was typical of a carbonate site (CO_3), presenting one narrow peak (290 eV) and one broad peak (300 eV), which corresponded to C=O (1s→π*) and C–O (1s→σ*) bonds, respectively, of the carbonate crystal. A small CK pre-peak at 285 eV may indicate the presence of small amounts of amorphous carbon. This, along with the electron diffraction patterns suggesting a monocrystalline structure, seemed at odds with what was shown by FEG-SEM, calling for a deeper investigation of the composition of the whole structure of spicules. By characterizing the morphology of the biomaterial at different length scales, this work facilitated the identification of specific textures and interfaces inside the bulk, thereby contributing to new knowledge.

Elongated calcium carbonate crystals are present in the hard parts of several organisms, such as calcareous sponges [23] and chitons [24]. Interestingly, it has been shown that under confinement, calcium carbonate mineralization favors the growth of aragonite at room temperature [25] and that magnesium cations may act as modifiers of the crystal habits of calcium carbonates [26]. Zeng et al. [25] also reported a preferential growth of aragonite crystals at room temperature inside cylindrical pores directly (diameters smaller than 25 nm) or in the presence of magnesium and sulfur (diameters of 200 nm). We thus hypothesized that the mineralization of spicules could also be influenced by geometrical constraints. An evaluation of the role of Sr and Mg associated with geometrical constraints of the matrix and/or temperature in vivo is still lacking [26]. Given that spicules from Caudofoveata mollusks initiate growth extracellularly on a cup-like organic template, we propose that they could serve as a biomineralization research model to perform this evaluation. Although, in general in this research, the dimensions of the organic template where spicules were formed were larger than the dimensions described by Zeng et al. [25], the spicules had different dimensions along the body *Falcidens* sp. The elementary compositions in the spicules throughout the body could help elucidate the dynamics of their formation and interaction with the environment. One example of this interaction was the presence of Sr in the spicule. This illustrates the dynamics of spicule development and the capacity of this organelle to detect the presence of this cation in the environment.

The understanding of molluscan early evolution and the phylogenetic relationships within the phylum has progressed significantly over the last decades [27–31]. Aplacophorans, shell-less worm-shaped mollusks (composed of Solenogastres and Caudofoveata) have been typically regarded as a sister group of the remaining mollusks. Many competing evolutionary proposals exist, roughly divided into those that include aplacophorans with a general plesiomorphic morphology and distinct relationship scenarios with remaining mollusks [32,33], and those where aplacophorans and chitons (polyplcophora) are considered to belong to the clade called Aculifera. The clade Aculifera would be a sister taxon of the Conchifera, the remaining mollusks [34–37]. Analyzing the microstructure and composition of the Caudofoveatan spicules may provide the structural basis for understanding the evolutionary patterns of biomineralization in mollusks and help future research on deep molluscan phylogeny.

Supplementary Materials: The following are available online at https://www.mdpi.com/article/10.3390/min13060750/s1, Figure S1. Image of *Falsidens* sp obtained with a stereoscope.; Figure S2. Topographic analysis of the dorsal face of *Falcidens* sp. spicule by AFM.; Figure S3. Topographic analysis of the dorsal face of *Falcidens* sp. spicule by AFM in a section plane perpendicular to the one in Figure S2. Figure S4. AFM image ("force image" obtained at "constant height") of the dorsal surface of a *Falcidens* sp. spicule. Figure S5. Electron microscopy analysis of a lamella obtained by FIB-SEM from an epoxy resin embedded spicule. Figure S6. Diffraction patterns obtained from a lamella in different orientations/zone axes, determined by the use of the goniometer. Table S1. Angles between oblique faces, measured directly from the AFM image in Figure S3.

Author Contributions: Conceptualization, M.F. and C.W.; methodology, C.W., A.L.R., J.C., C.D.d.C.O., C.A., J.W. and M.F.; investigation, C.W., A.L.R., J.C., C.D.d.C.O., C.A., J.W. and M.F.; resources, M.F.; writing—original draft preparation, M.F. and C.W.; writing—review and editing, A.L.R.; supervision, M.F.; funding acquisition, M.F. All authors have read and agreed to the published version of the manuscript.

Funding: This research was funded by the Brazilian agencies CAPES, CNPq, and FAPERJ.

Data Availability Statement: Not applicable.

Acknowledgments: We acknowledge Flavio Passos and Marcel Miranda, from Universidade Estadual de Campinas and Bechara Kachar (NIDCD-NIH) for the exchange of ideas. This work is dedicated to Ulysses Lins and Renato Cruz, both in memoriam. The authors thank LABNANO/CBPF for its support during lamella preparation and TEM analysis.

Conflicts of Interest: The authors declare no conflict of interest.

References

1. Crenshaw, M.A. Biomineralization Mechanisms. In *Skeletal Biomineralization:Patterns, Processes, and Evolutionary Trends*; Carter, J.G., Ed.; Springer: New York, NY, USA, 1991; p. 302.
2. Lowenstam, H.A.; Weiner, S. *On Biomineralization*; Cambridge University Press: New York, NY, USA, 1989.
3. Bøggild, O.B. The Shell Structure of the Mollusks. *Dan. Vidensk. Selsk. Skr. Naturvidensk. Math. Afd.* **1930**, *9*, 231–326.
4. Kobayashi, I. Internal Microstructure of the Shell of Bivalve Molluscs. *Am. Zool.* **1969**, *9*, 663–672. [CrossRef]
5. Mastropietro, F.; Godard, P.; Burghammer, M.; Chevallard, C.; Daillant, J.; Duboisset, J.; Allain, M.; Guenoun, P.; Nouet, J.; Chamard, V. Revealing Crystalline Domains in a Mollusc Shell Single-Crystalline Prism. *Nat. Mater.* **2017**, *16*, 946–952. [CrossRef] [PubMed]
6. Giles, R.; Manne, S.; Mann, S.; Morse, D.E.; Stucky, G.D.; Hansma, P.K. Inorganic Overgrowth of Aragonite on Molluscan Nacre Examined by Atomic Force Microscopy. *Biol. Bull.* **1995**, *188*, 8–15. [CrossRef] [PubMed]
7. Walker, J.M.; Marzec, B.; Ozaki, N.; Clare, D.; Nudelman, F. Morphological Development of Pleurochrysis Carterae Coccoliths Examined by Cryo-Electron Tomography. *J. Struct. Biol.* **2020**, *210*, 107476. [CrossRef] [PubMed]
8. Dauphin, Y.; Dufour, E. Nanostructures of the Aragonitic Otolith of Cod (*Gadus morhua*). *Micron* **2008**, *39*, 891–896. [CrossRef] [PubMed]
9. Beedham, G.E.; Trueman, E.R. The Cuticle of the Aplacophora and Its Evolutionary Significance in the Mollusca. *J. Zool.* **1968**, *154*, 443–451. [CrossRef]
10. Haas, W. Evolution of Calcareous Hard Parts in Primitive Molluscs. *Malacologia* **1981**, *21*, 403.
11. Scheltema, A.H.; Tscherkassky, M.; Kuzirian, A.M. Aplacophora. In *Microscopic Anatomy of Invertebrates. Mollusca I*; Harrison, F.W., Kohn, A.J., Eds.; Wiley-Liss: New York, NY, USA, 1994; pp. 13–54.
12. Mikkelsen, N.; Todt, C. Diversity of Caudofoveata (Mollusca) Around Iceland and Description of *Psilodens Balduri* sp. n. *Polish Polar Res.* **2014**, *35*, 279–290. [CrossRef]
13. Señarís, M.P.; García-Álvarez, O.; Urgorri, V. Four New Species of Chaetodermatidae (Mollusca, Caudofoveata) from Bathyal Bottoms of the NW Iberian Peninsula. *Helgol. Mar. Res.* **2016**, *70*, 28. [CrossRef]
14. Dalboni, L.C.; Coelho, C.D.P.C.D.P.; Palombo Pedro, R.R.R.R.; Correia, M.S.M.S.; De Santana, F.R.F.R.; Cardoso, T.N.T.N.; Pinto, S.A.G.S.A.G.; Alvares-Saraiva, A.M.A.M.; Dutra-Correa, M.; Peres, G.B.G.B.; et al. Biological Actions, Electrical Conductance and Silicon-Containing Microparticles of Arsenicum Album Prepared in Plastic and Glass Vials. *Homeopathy* **2019**, *108*, 12–23. [CrossRef] [PubMed]
15. Scheltema, A.H. The Aplacophoran Family Prochaetodermatidae in the North American Basin, Including *Chevroderma n.g.* and *Spathoderma n.g.* (Mollusca; Chaetodermomorpha). *Biol. Bull.* **1985**, *169*, 484–529. [CrossRef] [PubMed]
16. Kingsley, R.J.; Froelich, J.; Marks, C.B.; Spicer, L.M.; Todt, C. Formation and Morphology of Epidermal Sclerites from a Deep-Sea Hydrothermal Vent Solenogaster (*Helicoradomenia* Sp., Solenogastres, Mollusca). *Zoomorphology* **2013**, *132*, 1–9. [CrossRef]
17. Srot, V.; Wegst, U.G.K.; Salzberger, U.; Koch, C.T.; Hahn, K.; Kopold, P.; van Aken, P.A. Microstructure, Chemistry, and Electronic Structure of Natural Hybrid Composites in Abalone Shell. *Micron* **2013**, *48*, 54–64. [CrossRef]
18. Kim, Y.-Y.; Schenk, A.S.; Ihli, J.; Kulak, A.N.; Hetherington, N.B.J.; Tang, C.C.; Schmahl, W.W.; Griesshaber, E.; Hyett, G.; Meldrum, F.C. A Critical Analysis of Calcium Carbonate Mesocrystals. *Nat. Commun.* **2014**, *5*, 4341. [CrossRef]
19. Mann, S. *Biomineralization: Principles and Concepts in Bioinorganic Materials Chemistry*; Oxford University Press: Oxford, UK, 2001; Volume 17, ISBN 0198508824.
20. Nudelman, F.; Gotliv, B.A.; Addadi, L.; Weiner, S. Mollusk Shell Formation: Mapping the Distribution of Organic Matrix Components Underlying a Single Aragonitic Tablet in Nacre. *J. Struct. Biol.* **2006**, *153*, 176–187. [CrossRef]
21. Walker, J.M.; Marzec, B.; Lee, R.B.Y.; Vodrazkova, K.; Day, S.J.; Tang, C.C.; Rickaby, R.E.M.; Nudelman, F. Polymorph Selectivity of Coccolith-Associated Polysaccharides from Gephyrocapsa Oceanica on Calcium Carbonate Formation in Vitro. *Adv. Funct. Mater.* **2019**, *29*, 1807168. [CrossRef]
22. Jehannin, M.; Rao, A.; Cölfen, H. New Horizons of Nonclassical Crystallization. *J. Am. Chem. Soc.* **2019**, *141*, 10120–10136. [CrossRef]
23. Rossi, A.L.; Ribeiro, B.; Lemos, M.; Werckmann, J.; Borojevic, R.; Fromont, J.; Klautau, M.; Farina, M. Crystallographic Orientation and Concentric Layers in Spicules of Calcareous Sponges. *J. Struct. Biol.* **2016**, *196*, 164–172. [CrossRef]
24. Treves, K.; Traub, W.; Weiner, S.; Addadi, L. Aragonite Formation in the Chiton (Mollusca) Girdle. *Helv. Chim. Acta* **2003**, *86*, 1101–1112. [CrossRef]

25. Zeng, M.; Kim, Y.-Y.; Anduix-Canto, C.; Frontera, C.; Laundy, D.; Kapur, N.; Christenson, H.K.; Meldrum, F.C. Confinement Generates Single-Crystal Aragonite Rods at Room Temperature. *Proc. Natl. Acad. Sci. USA* **2018**, *115*, 7670–7675. [CrossRef] [PubMed]
26. Fermani, S.; Njegić Džakula, B.; Reggi, M.; Falini, G.; Kralj, D. Effects of Magnesium and Temperature Control on Aragonite Crystal Aggregation and Morphology. *CrystEngComm* **2017**, *19*, 2451–2455. [CrossRef]
27. Sutton, M.D.; Briggs, D.E.; Siveter, D.J.; Siveter, D.J. An Exceptionally Preserved Vermiform Mollusc from the Silurian of England. *Nature* **2001**, *410*, 461–463. [CrossRef]
28. Kocot, K.M. Recent Advances and Unanswered Questions in Deep Molluscan Phylogenetics. *Am. Malacol. Bull.* **2013**, *31*, 195–208. [CrossRef]
29. Telford, M.J.; Budd, G.E. Invertebrate Evolution: Bringing Order to the Molluscan Chaos. *Curr. Biol.* **2011**, *21*, R964–R966. [CrossRef]
30. Scheltema, A.H. Phylogenetic Position of Sipuncula, Mollusca and the Progenetic Aplacophora. In *Origin and Evolutionary Radiation of the Mollusca*; Taylor, J., Ed.; Oxford London Press: Oxford, UK, 1996.
31. Smith, S.A.; Wilson, N.G.; Goetz, F.E.; Feehery, C.; Andrade, S.C.S.; Rouse, G.W.; Giribet, G.; Dunn, C.W. Resolving the Evolutionary Relationships of Molluscs with Phylogenomic Tools. *Nature* **2011**, *480*, 364–367. [CrossRef] [PubMed]
32. Haszprunar, G. Is the Aplacophora Monophyletic? A Cladistic Point of View. *Am. Malacol. Bull.* **2000**, *15*, 115–130.
33. Salvini-Plawen, L.V. On the Phylogenetic Significance of the Neurenteric Canal (Chordata). *Zoology* **1999**, *102*, 175–183.
34. Sutton, M.D.; Briggs, D.E.G.; Siveter, D.J.; Siveter, D.J.; Sigwart, J.D. A Silurian Armoured Aplacophoran and Implications for Molluscan Phylogeny. *Nature* **2012**, *490*, 94–97. [CrossRef]
35. Vinther, J.; Parry, L.; Briggs, D.E.G.; Van Roy, P. Ancestral Morphology of Crown-Group Molluscs Revealed by a New Ordovician Stem Aculiferan. *Nature* **2017**, *542*, 471–474. [CrossRef]
36. Kocot, K.M.; Todt, C.; Mikkelsen, N.T.; Halanych, K.M. Phylogenomics of Aplacophora (Mollusca, Aculifera) and a Solenogaster without a Foot. *Proc. Biol. Sci.* **2019**, *286*, 20190115. [CrossRef] [PubMed]
37. Scherholz, M.; Redl, E.; Wollesen, T.; Todt, C.; Wanninger, A. Aplacophoran Mollusks Evolved from Ancestors with Polyplacophoran-like Features. *Curr. Biol.* **2013**, *23*, 2130–2134. [CrossRef] [PubMed]